

Nanofibrous nerve guidance conduits decorated with decellularized matrix hydrogel facilitate peripheral nerve injury repair

Chushan Zheng^{1,2#}, Zehong Yang^{1,2#}, Shihao Chen^{3#}, Fang Zhang^{1,2}, Zilong Rao³, Cailing Zhao⁴, Daping Quan^{3,4}, Ying Bai^{4✉}, Jun Shen^{1,2✉}

1. Department of Radiology, Sun Yat-sen Memorial Hospital, Sun Yat-sen University, Guangzhou, Guangdong 510120, China.
2. Guangdong Provincial Key Laboratory of Malignant Tumor Epigenetics and Gene Regulation, Medical Research Center, Sun Yat-sen Memorial Hospital, Sun Yat-sen University, Guangzhou, Guangdong 510120, China.
3. PCFM Lab, GD HPPC Lab, School of Chemistry, Sun Yat-sen University, Guangzhou, Guangdong 510275, China.
4. Guangdong Functional Biomaterials Engineering Technology Research Center, School of Materials Science and Engineering, Sun Yat-sen University, Guangzhou, Guangdong 510275, China.

These authors contributed equally to this work.

✉ Corresponding authors: Ying Bai, baiy28@mail.sysu.edu.cn; School of Materials Science and Engineering, Sun Yat-sen University, 135 Xin'gang Xi Road, Guangzhou, Guangdong 510275, China. Jun Shen, shenjun@mail.sysu.edu.cn; Sun Yat-sen Memorial Hospital, Sun Yat-sen University, No. 107 Yanjiang Road West, Guangzhou, Guangdong 510120, China.

© The author(s). This is an open access article distributed under the terms of the Creative Commons Attribution License (<https://creativecommons.org/licenses/by/4.0/>). See <http://ivyspring.com/terms> for full terms and conditions.

Received: 2020.07.18; Accepted: 2020.12.21; Published: 2021.01.01

Abstract

Rationale: Peripheral nerve injury (PNI) is a great challenge for regenerative medicine. Nerve autograft is the gold standard for clinical PNI repair. Due to its significant drawbacks, artificial nerve guidance conduits (NGCs) have drawn much attention as replacement therapies. We developed a combinatorial NGC consisting of longitudinally aligned electrospun nanofibers and porcine decellularized nerve matrix hydrogel (pDNM gel). The *in vivo* capacity for facilitating nerve tissue regeneration and functional recovery was evaluated in a rat sciatic nerve defect model.

Methods: Poly (L-lactic acid) (PLLA) was electrospun into randomly oriented (PLLA-random) and longitudinally aligned (PLLA-aligned) nanofibers. PLLA-aligned were further coated with pDNM gel at concentrations of 0.25% (PLLA-aligned/0.25% pDNM gel) and 1% (PLLA-aligned/1% pDNM gel). Axonal extension and Schwann cells migration were evaluated by immunofluorescence staining of dorsal root ganglia cultured on the scaffolds. To fabricate implantable NGCs, the nanofibrous scaffolds were rolled and covered with an electrospun protection tube. The fabricated NGCs were then implanted into a 5 mm sciatic nerve defect model in adult male Sprague-Dawley rats. Nerves treated with NGCs were compared to contralateral uninjured nerves (control group), injured but untreated nerves (unstitched group), and autografted nerves. Nerve regeneration was monitored by an established set of assays, including T2 values and diffusion tensor imaging (DTI) derived from multiparametric magnetic resonance imaging (MRI), histological assessments, and immunostaining. Nerve functional recovery was evaluated by walking track analysis.

Results: PLLA-aligned/0.25% pDNM gel scaffold exhibited the best performance in facilitating directed axonal extension and Schwann cells migration *in vitro* due to the combined effects of the topological cues provided by the aligned nanofibers and the biochemical cues retained in the pDNM gel. Consistent results were obtained in animal experiments with the fabricated NGCs. Both the T2 and fractional anisotropy values of the PLLA-aligned/0.25% pDNM gel group were the closest to those of the autografted group, and returned to normal much faster than those of the other NGCs groups. Histological assessment indicated that the implanted PLLA-aligned/0.25% pDNM gel NGC resulted in the largest number of axons and the most extensive myelination among all fabricated NGCs. Further, the PLLA-aligned/0.25% pDNM gel group exhibited the highest sciatic nerve function index, which was comparable to that of the autografted group, at 8 weeks post-surgery.

Conclusions: NGCs composed of aligned PLLA nanofibers decorated with 0.25% pDNM gel provided both topological and biochemical guidance for directing and promoting axonal extension, nerve fiber myelination, and functional recovery. Moreover, T2-mapping and DTI metrics were found to be useful non-invasive monitoring techniques for PNI treatment.

Key words: decellularized nerve matrix hydrogel, peripheral nerve injury, nerve guidance conduit, magnetic resonance imaging, electrospinning

Introduction

Peripheral nerve injury (PNI) is a common clinical disease that leads to sensory and motor deficits. Neurotmesis, a complete transection or disruption of the entire nerve, is the most severe form of PNI. The long-distance defect/gap between the proximal and distal stumps of the damaged nerve often results in limited regeneration capacity [1, 2]. Autologous nerve grafting is the gold standard for clinical treatment of peripheral nerve defects [3]. However, the major drawbacks of nerve autografts, such as limited donor tissue, secondary body injury, repeated surgeries, and size/structural disproportion of grafted nerve tissue, are also significant [4, 5]. Artificial nerve guidance conduits (NGCs) were invented for bridging the two stumps of the defected nerves [6]. To date, a large variety of NGCs have been developed to overcome the disadvantages of nerve autografts and provide alternative therapeutic approaches for treatment of PNI [7]. However, most of the FDA-approved NGCs that consist of either biodegradable synthetic polymers or natural biomaterials (e.g., collagen) are only fabricated as single tubular structures [8, 9]. Generally, these conduits provide a large space for nerve fiber regeneration once sutured between the proximal and distal ends of the defect, but they also lead to axonal dispersion due to the lack of topological and biological guidance, which is inhibitory to nerve functional recovery [10, 11]. Therefore, rational selection of functional materials and smart design of microscopic architectures are both essential in current advancements of NGCs [6, 12].

Within the last decade, tissue-engineered nerve grafts have been developed from biomaterial-based scaffolds combined with additional growth factors [13] and other bioactive molecules [14] to trigger neurogenesis and facilitate restoration of neural functions [15, 16]. As a type of bioactive scaffold, decellularized extracellular matrix (dECM) derived from tissues or organs has attracted increasing attention due to its tissue specificity and preservation of the composition and microstructure of native extracellular matrix (ECM) [17, 18]. dECM is often more than a scaffold, serving as a functional regulator of cell differentiation, signal transduction, proliferation, morphogenesis, and remodeling in the

host [11]. Furthermore, many tissue-derived dECMs undergo enzymatic digestion to form dECM hydrogels via sol-gel transition [19-21]. For instance, decellularized nerve matrix hydrogel derived from porcine sciatic nerves (pDNM gel) was reported to effectively promote neurite remyelination but inhibit synaptogenesis in vitro [22].

Besides the bioactivity of the scaffolding material, major challenges in peripheral nerve regeneration involve misdirected axonal growth. It has been widely acknowledged that longitudinally aligned fiber-like or channel-like microstructures critically contribute to the guidance of neurite outgrowth [23-26]. Pioneering studies have also shown that aligned electrospun nanofibers can support oriented axonal extension and glial cells (Schwann cells, SCs) migration from cultured primary dorsal root ganglion (DRG) explants [27, 28]. Furthermore, in vitro studies suggest that longitudinally aligned nanofibers can accelerate neurite extension compared to nanofibers with random alignments [29-31]. Our previous study showed clear evidence that aligned nanofibers coated with pDNM gel can facilitate synergistic effects in directed axonal extension and SC migration in seeded DRG explants [32]. We demonstrated that pDNM gel-accelerated SC migration can further promote and guide neurite outgrowth along the aligned nanofibers. However, whether composite pDNM gel-coated nanofibrous scaffolds contribute to nerve regeneration and functional recovery in a PNI animal model remains to be evaluated.

Herein, longitudinally aligned poly (*L*-lactic acid) (PLLA) nanofibers were precoated with pDNM gel and fabricated into tissue-engineered NGCs with electrospun protection tubes. These prepared nanofiber NGCs were implanted into a defected sciatic nerve rat model. The performance of these implanted NGCs was evaluated in comparison with the contralateral uninjured side (control group), untreated injured nerves (unstitched group), as well as autografted nerves. Magnetic resonance imaging (MRI) is a powerful noninvasive diagnostic tool for assessing PNI and nerve tissue regeneration via direct visualization of peripheral nerve changes [31]. Quantitative MRI parameters, including T2 values

and metrics of diffusion tensor imaging (DTI), can sensitively detect the continuity of neurites and indicate the extent of nerve dysfunction/regeneration at various timepoints, such as immediately following acute PNI, during the recovery phase, and before regenerated axons reach their target [33-36]. In this study, sciatic nerve reinnervation in rats was assessed by multiparametric MRI and evaluated using T2-mapping and DTI. It was hypothesized that the combinatorial pDNM gel and aligned nanofibers scaffold could provide both biochemical and topological guidance for promoting axonal extension and functional recovery after PNI. Additionally, PNI repair could be monitored non-invasively and in situ by MRI.

Materials and Methods

Animals and ethics

All interventions and animal care procedures were performed following the Guidelines and Policies for Animal Surgery at Sun Yat-sen University (Guangzhou, China) and were approved by the Institutional Animal Use and Care Committee. 144 healthy adult male Sprague-Dawley (SD) rats (250 ± 20 g) were obtained from the Animal Experiment Centre of Sun Yat-sen University. The rodents were kept under a 12 h light/dark cycle with free access to food and water. The rats were transported and kept more than 7 days in advance of surgery.

Preparation of electrospun nanofibrous scaffolds

Poly (L-lactic acid) (PLLA; PURAC, Groningen, Holland) was dissolved in 2,2,2-trifluoroethanol (TFE) (Aladdin, Shanghai, China) to obtain a 7.5% (w/v) polymer solution, then transferred into a syringe with a 20G stainless steel needle. The polymer solution was ejected at 1 mL/h by a syringe pump (Tonli, Shenzhen, China). To collect PLLA nanofibers, a high voltage power supply (Tonli, Shenzhen, China) was connected to the needle and set to 15 kV. The randomly oriented nanofibers were collected on clean glass slides on top of a steel plate. The distance between the needle and the collection plate was 100 mm. To produce longitudinally aligned nanofibers, a roller wheel with pre-attached glass coverslips was used as the collector with a rotational speed of 3000 rpm. After 20 min of nanofiber collection, the samples were vacuum-dried for 24 h to remove residual solvent.

Decellularized nerve matrix hydrogel coating

Decellularized matrix hydrogel derived from porcine sciatic nerves (pDNM gel) was prepared following our previously reported protocols [34, 37].

Briefly, fresh sciatic nerves harvested from miniature pigs were extracted with 3.0% Triton X-100 and 4.0% sodium deoxycholate and rinsed with sterile water three times until completely decellularized. The decellularized pDNM was lyophilized, pulverized into a powder, then solubilized in acidic pepsin solution (0.01 M HCl) to 1% (w/v) pDNM and 10/1 (w/w) pDNM/pepsin at room temperature for 24 h. The digested solution was centrifuged at 20,000 rpm (Beckman Coulter, Brea, USA) for 30 min to remove all undissolved contents, lyophilized and then pulverized to powder. The powder was re-dissolved in 0.01 M HCl to 2% (w/v), the pH was adjusted to 7.5 by addition of 0.1 M NaOH, and 10× PBS was added to form pDNM-sol. The sol was diluted to 0.25% (w/v) and 1% (w/v) with 1× PBS.

The aligned PLLA nanofibrous films were pre-sterilized with 75% ethanol, immersed in 0.25% (w/v) or 1% (w/v) pDNM-sol for 10 min at 4 °C, then gelled at 37 °C for 20 min. The films were then lyophilized and stored at -40 °C before use. All solutions used were sterile, and all above-mentioned procedures were performed in a sterilized environment.

Preparation of NGCs

Electrospun poly (L-lactic acid-co-trimethylene carbonate) P(LLA-TMC) nanofibers (LLA/TMC = 70/30) were used to fabricate the protection tubes of the implantable NGCs. PLLA-random, PLLA-aligned, PLLA-aligned/0.25% pDNM gel, or PLLA-aligned/1% pDNM gel scaffolds were first wrapped around a stainless steel rod (diameter = 2 mm) to serve as the collection substrates for electrospun P(LLA-TMC) nanofibers. P(LLA-TMC) tubes were fabricated from 15% (w/v) P(LLA-TMC) in TFE. The solution was ejected onto the collection substrates through a 0.65 mm needle charged at 15 kV and dispensed at a flow rate of 0.5 mL/h. The total length of each NGC was 10 mm.

DRG culture and immunofluorescence staining

The scaffolds were immersed in 75% ethanol for 30 min and washed with PBS three times for sterilization. DRGs were dissected from newborn SD rats (postnatal day 1, supplied by the Laboratory Animal Center of Sun Yat-sen University, China). Residual nerve roots were cut off under a stereomicroscope. Then, the isolated DRGs were plated on PLLA nanofibrous films with or without pDNM-gel coating, placed in 48-well plates with neurobasal medium containing 2% B27, 0.3% L-glutamine, and 1% penicillin-streptomycin, and incubated at 37 °C in 5% CO₂ and 92% humidity. The medium was changed every 2 days.

After culturing for 7 days, the samples were fixed in 4% paraformaldehyde in PBS for 20 min, rinsed with PBS, and permeabilized and blocked in 0.1% Triton X-100 and 10% donkey serum in PBS for 30 min. DRG samples were incubated with primary antibodies against NF200 (dilution 1/150) or S100 (dilution 1/1000) for 2 h at room temperature, followed by secondary antibodies conjugated to Fluro-488 (dilution 1/1000) or Fluro 594 (dilution 1/1000) for 1h. The samples were then rinsed with PBS for 10 min (3 times), stained with DAPI (dilution 1/2500) for 20 min, then observed by a laser scanning confocal microscope (Zeiss, Germany).

Animal surgery and NGC implantation

Animals were randomly selected and placed into two groups. Each group was subdivided into six subgroups: autografted, unstitched, PLLA-random, PLLA-aligned, PLLA-aligned/0.25% pDNM gel, and PLLA-aligned/1% pDNM gel ($n = 6$ per subgroup in the first group, and $n = 18$ per subgroup in the second group). Following a previously reported procedure [35, 38], general anesthesia was administered by intraperitoneal injection of pentobarbital sodium (40 mg/kg) after isoflurane inhalation. Then, the animals were placed in a prone position. A 20 mm incision was made along the left femoral axis to separate the thigh muscles with the sciatic nerve dissected. The sciatic nerve was exposed, and its middle portion was removed to create a 5 mm gap between the proximal and distal stumps. For the autografted group, the transected 5 mm sciatic nerve was reversed and then grafted back using 8-0 sutures (Prolene; Jinhuan Medical Appliance, Shanghai, China) [39, 40]. For the unstitched group, no further treatment was performed after the 5 mm sciatic nerve segment was excised. For the groups implanted with NGCs, the fabricated NGCs were implanted to bridge the proximal and distal ends of the nerve defects. Both nerve stumps were inserted into the tube lumen (depth = ~2 mm) and sutured to the conduit wall using a single epineurial 8-0 suture. The wounds were then closed, and the animals were returned to their cages [38].

The animals in the first group underwent MRI and sciatic nerve functional assessments at 1, 2, 6, and 8 weeks post-surgery. The rats in the second group were subjected to histologic analysis at 2, 6, and 8 weeks post-surgery. The uninjured nerve on the contralateral side of each animal was used as the control group.

MRI acquisition and evaluation

MRI was performed on a 3.0 T scanner (Achieva; Philips Medical Systems, Best, Netherlands) with a 50

mm × 50 mm 4-channel phased-array rat coil (Chenguang Medical Technologies Co., Shanghai, China). After anesthesia, animals were placed in a supine position. Coronal fat-suppressed turbo spin-echo T2-weighted imaging (FS-T2WI), T2 mapping, and axial DTI data were acquired. Parameters of acquisition for FS-T2WI were as follows: repetition time (TR) = 1200 ms, echo time (TE) = 60 ms, acquisition matrix = 172 × 170, reconstruction matrix = 256 × 256, field of view (FOV) = 60 mm × 60 mm, number of signals averaged (NSA) = 1, and slice thickness/gap = 1 mm / 0 mm. T2 mapping was obtained using a multi-slice, multi-echo spin-echo sequence with the following parameters: TR = 1600 ms, TE = 20–160 ms, matrix = 148 × 171, FOV = 60 mm × 60 mm, NSA = 2, and slice thickness/gap = 2 mm / 0 mm. Axial DTI was obtained using an echoplanar imaging (EPI) sequence with the following acquisition parameters: TR = 1206 ms, TE = 79 ms, slice thickness/gap = 1.5 mm / 0.5 mm, b-value = 0.800 s/mm², 16 gradients, FOV = 60 mm × 128 mm, NSA = 2, acquisition matrix = 76 × 56, voxel size = 1.6 mm, reconstruction matrix = 256 × 256, reconstruction voxel size = 0.188 mm, EPI factor = 7, and flip angle = 90°. The imaging plane was parallel to the longitudinal course of the sciatic nerve for coronal images and perpendicular to the sciatic nerve (covering the lesion epicenter and proximal and distal stumps) for DTI.

Image analysis

Morphological abnormalities were assessed by FS-T2WI. Fractional anisotropy (FA) values were derived from DTI images of the distal stumps of injured nerves. T2 and FA values in regions of interest (ROI) were calculated from T2-mapping and DTI images on a workstation (View Forum; Philips) [38]. Briefly, a rectangular ROI with a minimum size of 85 pixels was placed within the implanted NGCs. To reduce partial volume effects, images demonstrating the long axis of sciatic nerves were chosen and the ROI position was carefully adjusted to the middle of the NGCs and covering the nerve trunk. The ROIs for DTI metrics were manually traced in the implanted conduits on axial DWI images for quantitation of FA. To ensure accurate and consistent positioning of the ROIs, transverse DTI images were linked with coronal T2-weighted images. ROI was manually selected and placed on three adjacent levels, which covered the whole injured site or its contralateral side (length = ~6 mm). The measurements were performed independently and blindly by two radiologists. The diffusion tensor was calculated on a pixel-by-pixel basis to obtain the eigenvectors and values. FA values were derived for each voxel [40–42]. Average values

from the 2 datasets were used for analysis. Tractography was obtained using the fiber tracking analysis software available on the same workstation. A multiple ROI method was used to reconstruct diffusion tensor tractography (DTT) [43]. Briefly, multiple ROIs were manually placed on each DTI axial image slice along the injured sciatic nerve from the proximal stump to the distal stump. Fibers passing through the multiple ROIs were visualized. The threshold of FA was set to 0.4, the maximum fiber angle was 27°, and the minimum fiber length was 15 mm [42].

Histology

At 2, 6, and 8 weeks after surgery, 6 animals in each group were euthanized and transcardially perfused with PBS to remove red blood cells. For the groups implanted with NGCs and the autografted group, the distal portions, the nerve grafts along the same severed nerves, and the sham-operated nerves were harvested. For the unstitched group, only the distal portions and the sham-operated nerves were harvested. The morphologies of the implanted NGCs and the nerve connections inside the tubes were observed under an optical microscope. Then, each tissue sample was split into two parts from the center of the nerve and fixed in 4% paraformaldehyde. Contiguous 1 μm cross-sections were obtained and stained with toluidine blue [44, 45]. The rest was longitudinally sectioned in 10 μm slices and immunofluorescence stained for small proline-rich protein 1A (SPRR1A) (Abcam, Cambridge, UK) to detect axonal regeneration [44]. The sample slices were rinsed in PBS, incubated in 0.3% Triton X-100 (Abcam, Cambridge, UK) for 15 min, blocked with donkey serum (10:100 (v/v); Abcam) for 30 min, then incubated overnight at 4 °C with primary antibodies against SPRR1A (1:200 (v/v); Abcam). After rinsing another three times with PBS, slices were incubated with the corresponding Alexa Fluor 488-conjugated secondary antibodies (1:200 v/v; Invitrogen, Carlsbad, USA) at room temperature for 1 h and subsequently with DAPI for nuclei staining. The immunostained samples were observed using a laser scanning confocal microscope (LSM780; Carl Zeiss, Jena, Germany).

For quantification of toluidine blue staining, the entire cross-sectional area of the injured nerve (1360 × 1024 pixels, 15.5 pixels/μm) was observed using the 1000× oil lens of an optical microscope (Olympus BX63; Olympus, Tokyo, Japan). The center and distal parts of the nerve grafts were selected for imaging. Five different regions in each part of the injured nerve (area = 5797 μm² per image, total area = 28,983 μm²) were randomly selected for analysis [35, 41]. The

number of axons, myelin thickness, and myelinated fiber diameter were measured using ImageJ (National Institutes of Health, Bethesda, Maryland).

Functional recovery assessment

Walking track analysis was performed for the first group of animals at each time point prior to MRI to assess nerve functional recovery by two experimenters in consensus. Sciatic nerve function index (SFI), an indicator of locomotor nerve dysfunction, was scored using the following parameters: normal print length (NPL), normal toe spread (NTS), normal intermediary toe spread (NIT), experimental print length (EPL), experimental toe spread (ETS), and experimental intermediary toe spread (EIT). SFI was calculated using the following formula [41]:

$$\text{SFI} = -38.3(\text{EPL} - \text{NPL})/\text{NPL} + 109.5(\text{ETS} - \text{NTS})/\text{NTS} + 13.3(\text{EIT} - \text{NIT})/\text{NIT} - 8.8$$

Statistical analysis

Repeated-measures one-way analysis of variance was used to evaluate the significance of T2, FA, and SFI values among the subgroups in the first group of animals, who underwent MRI and functional recovery assessments. Interobserver agreement and statistical power were also assessed. The T2, FA, and SFI values were compared between these subgroups using a Bonferroni test for multiple pairwise comparisons at each time point (1, 2, 6, and 8 weeks post-surgery) to determine the effect of pDNM gel concentration. Toluidine blue staining results were compared between subgroups in the second group of animals, who were subjected to histologic analysis, using one-way analysis of variance followed by a Bonferroni post-hoc test for multiple pairwise comparisons. Statistical analyses were performed using SPSS version 25.0 for Mac (SPSS, Inc., Chicago, Illinois). All data are presented as mean ± standard deviation. A 2-sided $p < 0.05$ was considered a significant difference.

Results

Fabrication of pDNM gel-decorated nanofibrous NGCs

Each implantable NGC consisted of two parts: an inner pDNM gel-coated or non-coated electrospun PLLA nanofibrous mesh and an outer P(LLA-TMC) protection tube. PLLA nanofibers were first obtained by electrospinning. These nanofibers were either randomly oriented (PLLA-random, Figure 1A) or longitudinally aligned (PLLA-aligned, Figure 1B) in 2D meshes. PLLA-aligned were then coated with pDNM gel at two different pDNM gel concentrations,

which resulted in two distinct morphologies on the upper surface. When PLLA-aligned were decorated with 0.25% (w/v) pDNM gel (PLLA-aligned/0.25% pDNM gel, Figure 1C), large PLLA nanofibers (diameter = ~650 nm) were easily visualized by scanning electron microscopy (SEM) and were associated with much smaller nanofibrous structures (30–50 nm), which is attributable to collagen fiber assembly in the pDNM gel. When 1% (w/v) pDNM gel was applied (PLLA-aligned/1% pDNM gel, Figure 1D), the dECM hydrogel fully covered the surface of the electrospun mesh and the nanofibrous topography was hardly identifiable by SEM, which is consistent with our previous findings [32]. The PLLA nanofibrous meshes, with or without pDNM gel coatings, were carefully wrapped around a stainless steel rod (diameter = 2 mm), then used as the collector for fabrication of electrospun P(LLA-TMC)70/30 protection tubes (illustrated in Figure 1E). The protection tubes possessed much denser fibers, which provides mechanical support, scaffold protection, and suturing capability (Figure 1F-G; microscopic morphology characterization, Figure S1; mechanical

characterization, Figure S2).

Nerve guidance of DRG explants in vitro

The nerve guidance effect of each nanofibrous scaffold was examined by DRG culture. Regenerating axons (NF200+) grew radially from seeded DRG explants when cultured on PLLA-random and PLLA-aligned/1% pDNM gel scaffolds, indicating an absence of topological guidance (Figure 2A, D). In comparison, neurite outgrowth was highly oriented along the electrospun nanofibers in both the PLLA-aligned and PLLA-aligned/0.25% pDNM gel groups, with integration of pDNM gel leading to much longer and thicker neurites (Figure 2B-C). Similar trends were observed for Schwann cells (S100+) migration on the fabricated scaffolds, with a larger number of Schwann cells migrating further on the pDNM gel-coated scaffolds than on the PLLA alone meshes (Figure S3). These *in vitro* results are consistent with our previous findings [23], but their outcomes on nerve regeneration and functional recovery still remain to be evaluated *in vivo*.

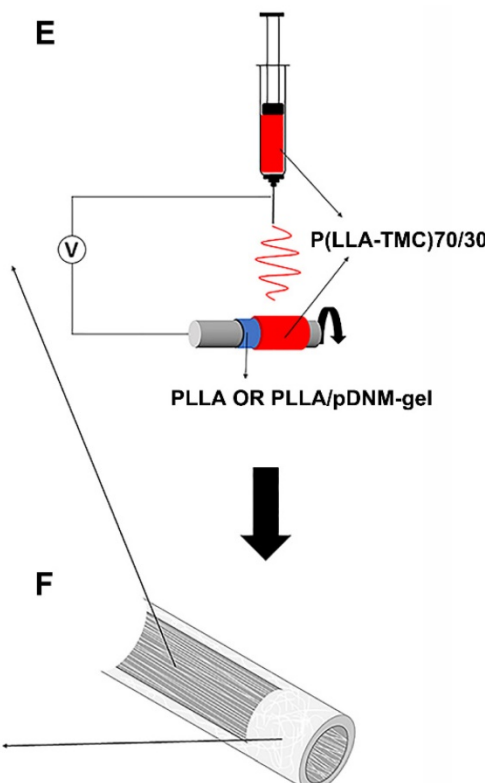
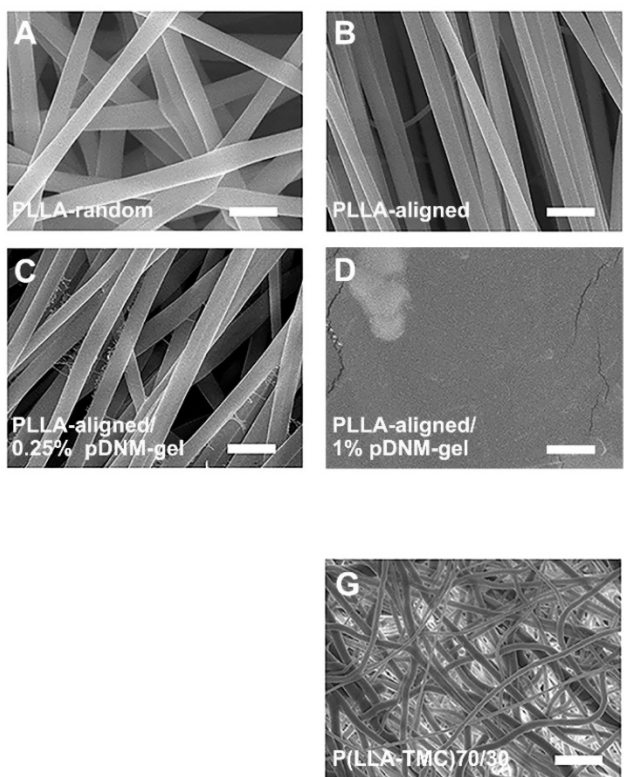


Figure 1. pDNM gel-coated electrospun nanofibrous scaffolds and NGC fabrication. Representative SEM micrographs of (A) randomly oriented electrospun PLLA nanofibers scaffolds (PLLA-random), (B) longitudinally aligned PLLA nanofibers scaffolds (PLLA-aligned), (C) PLLA-aligned scaffolds coated with 0.25% (w/v) pDNM gel (PLLA-aligned/0.25% pDNM gel), and (D) PLLA-aligned scaffolds coated with 1% (w/v) pDNM gel (PLLA-aligned/1% pDNM gel). Scale bars = 2 μ m. (E) Schematic illustration of the fabrication process for P(LLA-TMC)70/30 protection tubes. The prepared nanofibrous PLLA scaffolds (with or without pDNM gel) were wrapped around a stainless-steel rod (diameter = 2 mm), then P(LLA-TMC)70/30 was electrospun onto and wrapped around the scaffolds. (F) Diagram of the fabricated NGCs illustrating the inner scaffold of electrospun PLLA nanofibers with or without pDNM gel coating and the outer protection tube consisting of dense P(LLA-TMC)70/30 nanofibers. (G) SEM image of P(LLA-TMC)70/30 nanofibers in the protection tubes. Scale bar = 10 μ m.

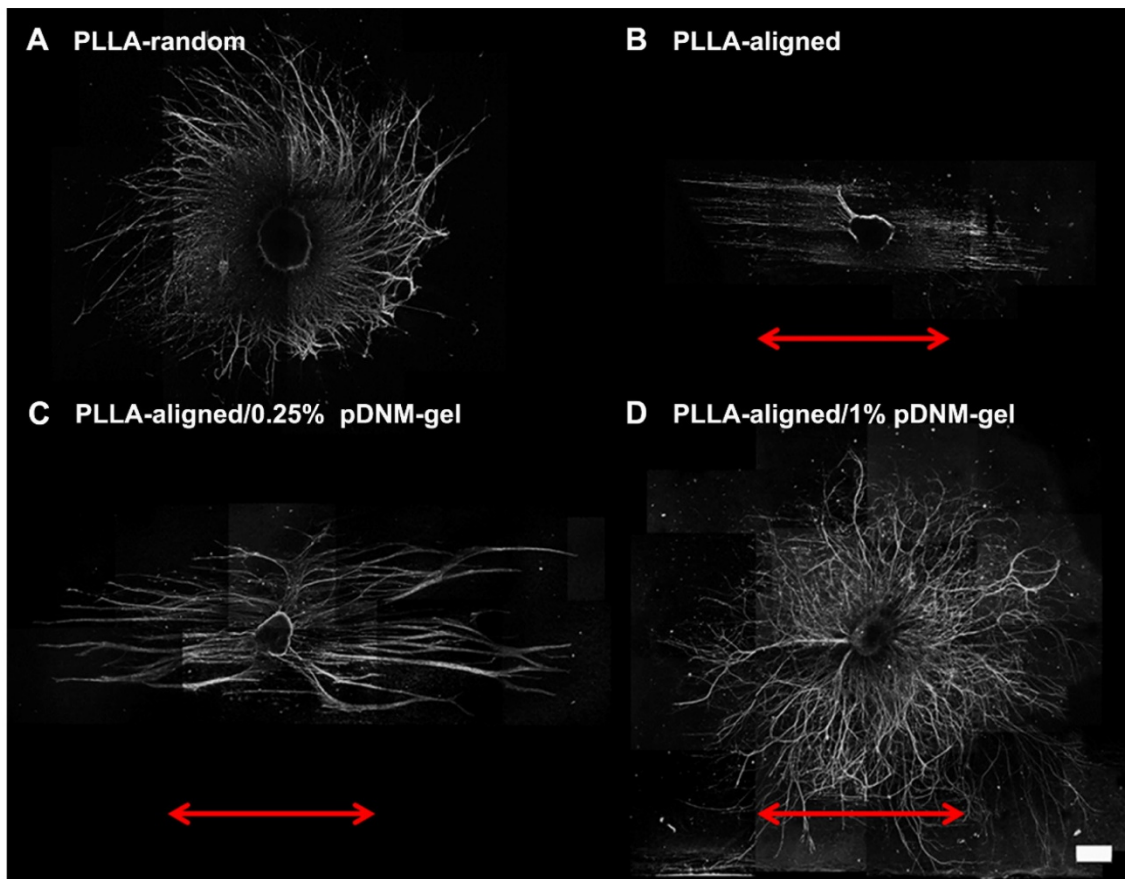


Figure 2. Immunofluorescence images showing neurite sprouting and extension from DRG explants. DRG explants were cultured on (A) PLLA-random, (B) PLLA-aligned, (C) PLLA-aligned/0.25% pDNM gel, or (D) PLLA-aligned/1% pDNM gel scaffolds. The red arrows indicate the direction of aligned nanofibers. The DRG explants were cultured for 7 days and immunostained for NF200. Scale bar = 500 μ m.

MRI monitoring of PNI repair *in vivo*

After surgery, the transected sciatic nerves in the unstitched group, the grafted sciatic nerves of the groups implanted with NGCs, and the autografted nerves were clearly visualized by FS-T2WI (Figure 3A). The uninjured nerves on the contralateral side served as the control group. The distal stumps of the injured nerves exhibited obviously enlarged and hyperintense T2 signals in all groups at the first week after surgery, which gradually decreased. The T2 signals of the autografted group and the PLLA-aligned/0.25% pDNM gel group returned to normal (similar to the uninjured nerves) at 6 weeks post-operation, while the groups implanted with the other NGCs took 8 weeks to return to normal. The T2 signals of the injured nerves in the unstitched group remained discontinuous two months after surgery.

The time dependence of the T2 values in the distal stumps of the injured nerves varied across the unstitched, autografted, PLLA-random, PLLA-aligned, PLLA-aligned/0.25% pDNM gel, and PLLA-aligned/0.25% pDNM gel groups (Figure 3B). Consistently, the T2 values of all groups implanted with NGCs and the autografted group increased

rapidly and reached similar peak values after one week. Afterwards, they decreased gradually but at different rates (slopes are given in Figure 3B). The T2 values of the autografted group and the PLLA-aligned/0.25% pDNM gel group reached their lowest levels in only 6 weeks, while the T2 values of the other injured groups continued to decrease for another two weeks. The T2 values of the autografted group were the lowest among all groups at 2 to 6 weeks post-operation. The T2 values of the PLLA-aligned group were lower than those of the PLLA-random group at 2 to 8 weeks. Additionally, the pDNM gel coating concentration influenced the T2 curves. The T2 values of the PLLA-aligned/0.25% pDNM gel group were significantly lower than those of the PLLA-aligned group at the second week post-surgery. However, the PLLA-aligned/1% pDNM gel group showed higher T2 values than the PLLA-aligned group within the same period, most likely due to the loss of topological guidance provided by the electrospun nanofibers. The T2 values of the unstitched group were the highest of all groups at 2 to 8 weeks and remained much higher than the normal level afterwards.

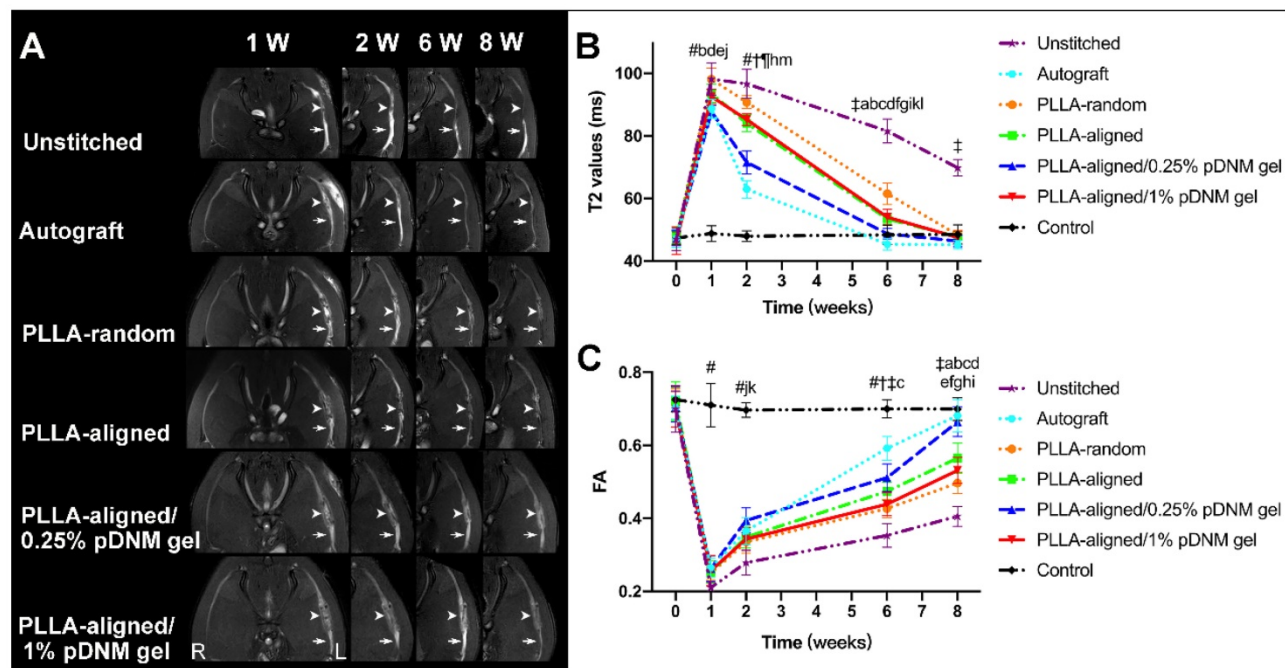


Figure 3. Sequential FS-T2WI of injured and contralateral uninjured sciatic nerves in rats. (A) MRI images showing the injured nerves on the left side of the unstitched, autografted, PLLA-random, PLLA-aligned, PLLA-aligned/0.25% pDNM gel, and PLLA-aligned/1% pDNM gel groups, and their corresponding uninjured nerves (control group) on the contralateral side. The injured nerves in all groups showed obviously enlarged and hyperintense signals in the proximal and distal portions, which gradually settled over time. The implanted NGCs (pointed out by arrowheads) were clearly delineated and hyperintense. R: right, L: left, W: week. **(B)** T2 values in the distal stumps of the injured nerves of all groups compared with their controls up to 8 weeks post-surgery. Statistically significant differences are listed in Table S2. **(C)** FA values in the distal stumps of the injured nerves of all groups compared with their controls up to 8 weeks post-surgery. Statistically significant differences are listed in Table S3.

The time dependence of the FA values followed opposite trends of the T2 values for all groups (Figure 3C). At 2 to 8 weeks after surgery, the FA values continued to increase, implying axonal regeneration within the injured nerves. Unlike the T2 values, the FA values of the injured nerves gradually approached but remained lower than those of the contralateral uninjured nerves at 8 weeks post-surgery. All the groups treated with aligned nanofibers, with or without pDNM gel coatings, exhibited larger FA values than those of the PLLA-random group at the first week after surgery. Among the groups treated with aligned nanofibers, the PLLA-aligned/0.25% pDNM gel group maintained the largest FA values at 2, 6, and 8 weeks post-operation, while the FA values of the PLLA-aligned/1% pDNM gel group were the lowest.

Compared with their contralateral uninjured nerves, the diameter of nerve tracts and the number of projected injured nerve fibers decreased 2 weeks after surgery, as characterized by DTT analysis (Figure 4). Thereafter, the morphology of all grafted nerves gradually recovered. The defected nerves almost returned to normal in the autografted group by 8 weeks post-operation. The PLLA-aligned/0.25% pDNM gel group showed more nerve fibers and larger nerve trajectories than the groups implanted with other NGCs at 2 to 8 weeks after surgery. The unstitched nerves remained discrete after surgery.

Histological characterization of nerve regeneration

Toluidine blue staining of the distal stumps of the injured nerves revealed massive axonal degeneration and myelin destruction 2 weeks post-operation. After treatment, significant progress in myelin debris clearance, axonal regeneration, and remyelination was identified in all groups at 6 and 8 weeks after surgery (Figure 5A). This was also evident within the injured portion (center region of the nerve grafts) at 8 weeks post-operation (Figure S4A). Statistically, the autografted group showed the largest number of axons (Figure 5B) as well as the most significant myelination effects at 6 and 8 weeks, including myelin thickness (Figure 5C) and myelinated nerve fiber diameter (Figure 5D), at the distal stumps among all injured groups, followed by the PLLA-aligned/0.25% pDNM gel group. Additionally, the PLLA-aligned/0.25% pDNM gel group showed the greatest number of axons and most significant myelination effects at the injured portion of the lesion sites among all the groups implanted with NGCs at 8 weeks (Figure S4B). Without pDNM gel, the topological guidance provided by the longitudinally aligned nanofibers in the PLLA-aligned group highly promoted nerve regeneration (axons count) and nerve fiber myelination (thickness of myelin and diameter of

myelinated fibers), compared to the PLLA-random group. Though incorporation of pDNM gel facilitates Schwann cells migration, the high gel concentration in the PLLA-aligned/1% pDNM gel group attenuated the topological guidance effects provided by the

electrospun nanofibers, which resulted in almost equivalent or even fewer regenerative axons and thinner myelin compared to the PLLA-aligned group (without pDNM gel) at 6 and 8 weeks post-surgery.

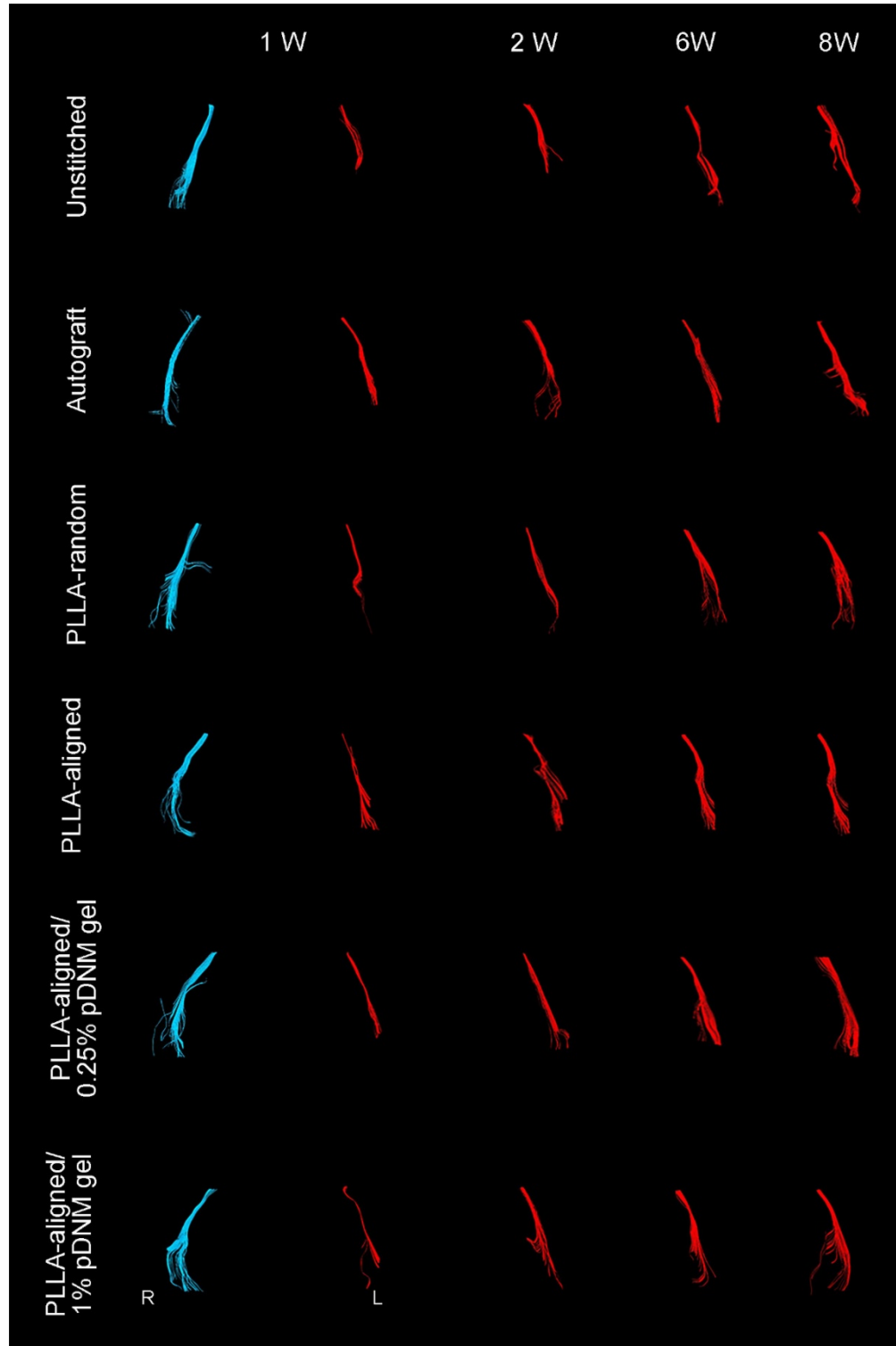


Figure 4. DTT of injured sciatic nerves (red) after surgery compared with uninjured nerves on the contralateral side (blue). Representative images showing the injured nerves on the left side of the unstitched, autografted, PLLA-random, PLLA-aligned, PLLA-aligned/0.25% pDNM gel, and PLLA-aligned/1% pDNM gel groups, and their corresponding uninjured nerves (control group) on the contralateral side. R: right, L: left, W: week.

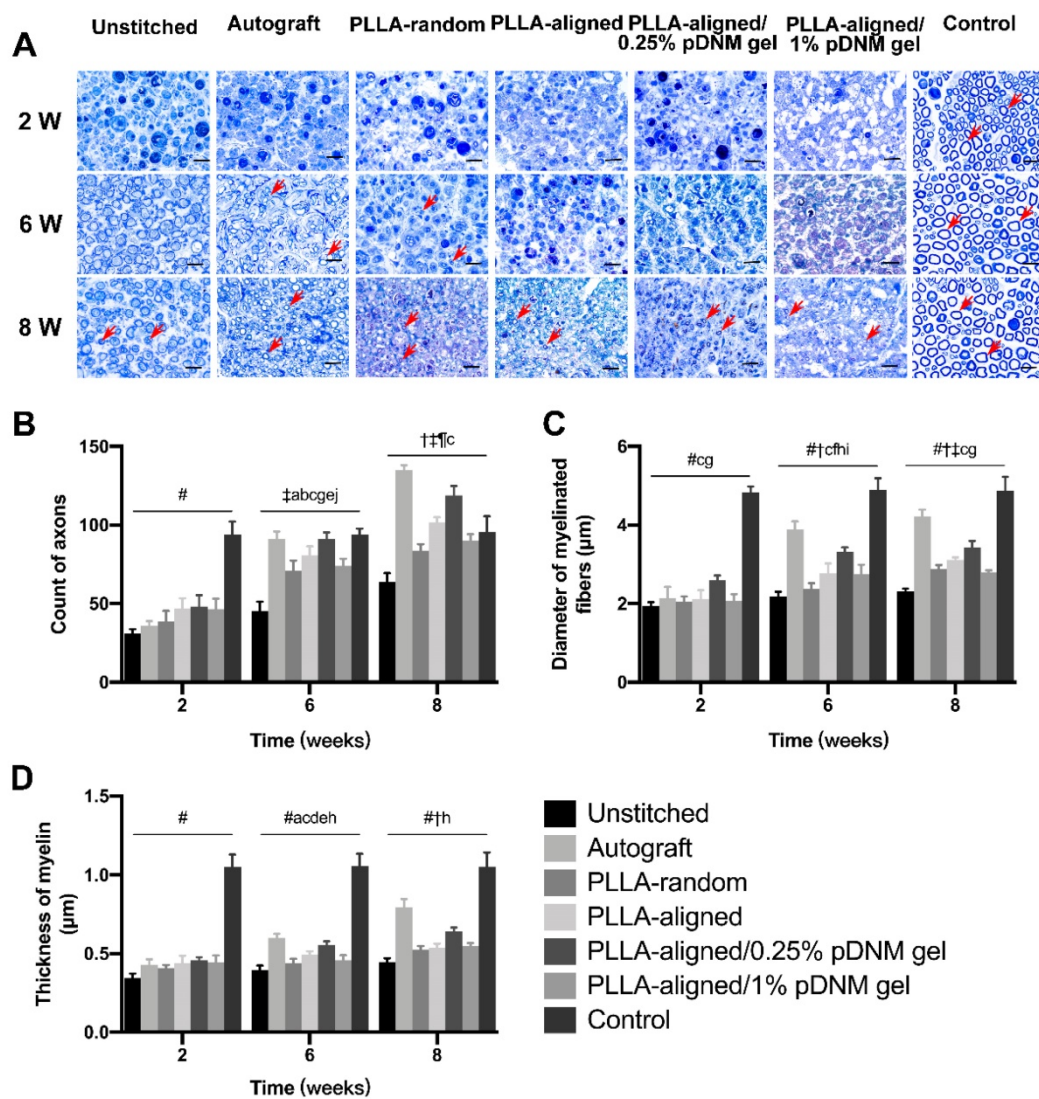


Figure 5. Toluidine blue staining of the distal stumps of injured and contralateral uninjured nerves. (A) Representative cross-sectional micrographs exhibiting axonal degeneration and myelin disintegration at 2 weeks post-surgery. The red arrowheads point out the myelinated axons. Pronounced axonal regeneration and remyelination were observed at 6 and 8 weeks post-operation, especially in the autografted group and the PLLA-aligned/0.25% pDNM gel group. W: week. Number of axons (**B**), myelin thickness (**C**), and diameter of myelinated nerve fibers (**D**) in the distal stumps of the injured nerves of all groups compared with their contralateral uninjured nerves (control group) at 2, 6, and 8 weeks post-surgery. Statistically significant differences are listed in Table S4.

The continuity of injured and regenerating nerve fibers was assessed by immunofluorescence staining using biomarker SPRR1A for regrowing axons (Figure 6). At the early stage after treatment (2 weeks post-operation), the nerve fibers were highly disordered at the injured sites of the unstitched, PLLA-random, PLLA-aligned, and PLLA-aligned/1% pDNM gel groups, but longitudinally aligned in the autografted and PLLA-aligned/0.25% pDNM gel NGCs groups. After 6 and 8 weeks of nerve repair, nerve fiber continuity was significantly improved in almost all the grafted groups. The autografted group showed the most promising recovery in nerve fiber continuity, while the unstitched group exhibited the most disconnected nerve fibers. The alignment of nerve fibers in the PLLA-aligned group was more obvious compared to that of the PLLA-random and

PLLA-aligned/1% pDNM gel groups. In comparison, in the PLLA-aligned/0.25% pDNM gel group, nerve fiber regrowth was closely packed and highly ordered, revealing the best performance in nerve regeneration. SPRR1A+ signal was minimal in the uninjured control group, since nerve fiber continuity was complete with very few growing axons.

Motor functional recovery

Finally, the motor function recovery of the injured rats was evaluated by walking track analysis and SFI. The hind paw footprints of the injured rats were recorded (Figure 7A). The injured animals displayed a sudden drop in SFI within the first week after surgery, which gradually recovered (Figure 7B). The SFI values kept increasing for all injured groups, with the autografted group possessing the highest SFI

value at 2 to 8 weeks after surgery, followed by the PLLA-aligned/0.25% pDNM gel group. The SFI values of the PLLA-random group were -81.7 ± 3.4 and -71.1 ± 3.6 at 6 and 8 weeks, respectively (Table S5), while those of the PLLA-aligned/1% pDNM gel group were -78.2 ± 5.5 and -66.8 ± 3.0 . The SFI values of these two groups were smaller than those of the

PLLA-aligned (-71.4 ± 6.3 and -59.9 ± 5.5) and PLLA-aligned/0.25% pDNM gel groups (-54.7 ± 4.6 and -44.9 ± 4.5). These results indicate that the grafted NGCs without topological fiber guidance (PLLA-random and PLLA-aligned/1% pDNM gel groups) provided much slower functional restoration at 6 and 8 weeks post-surgery.

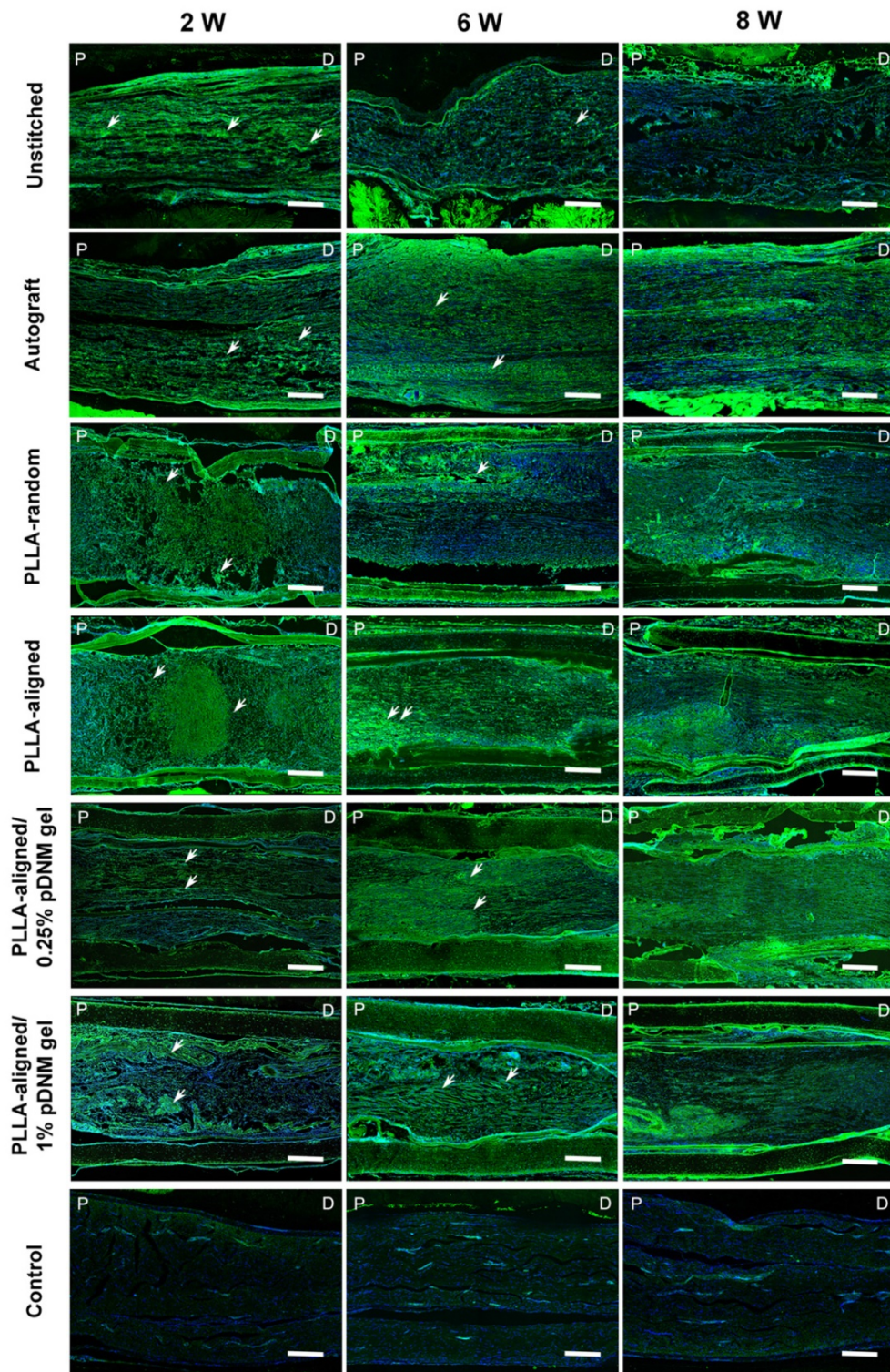


Figure 6. SPRR1A staining showing the continuity of regenerating nerve fibers. Representative images of regrowing axons from all groups, immunofluorescence stained with SPRR1A at 2, 6, and 8 weeks post-surgery. The white arrowheads point out the regrowing axons. P: proximal, D: distal, W: week. Scale bars = 300 μ m.

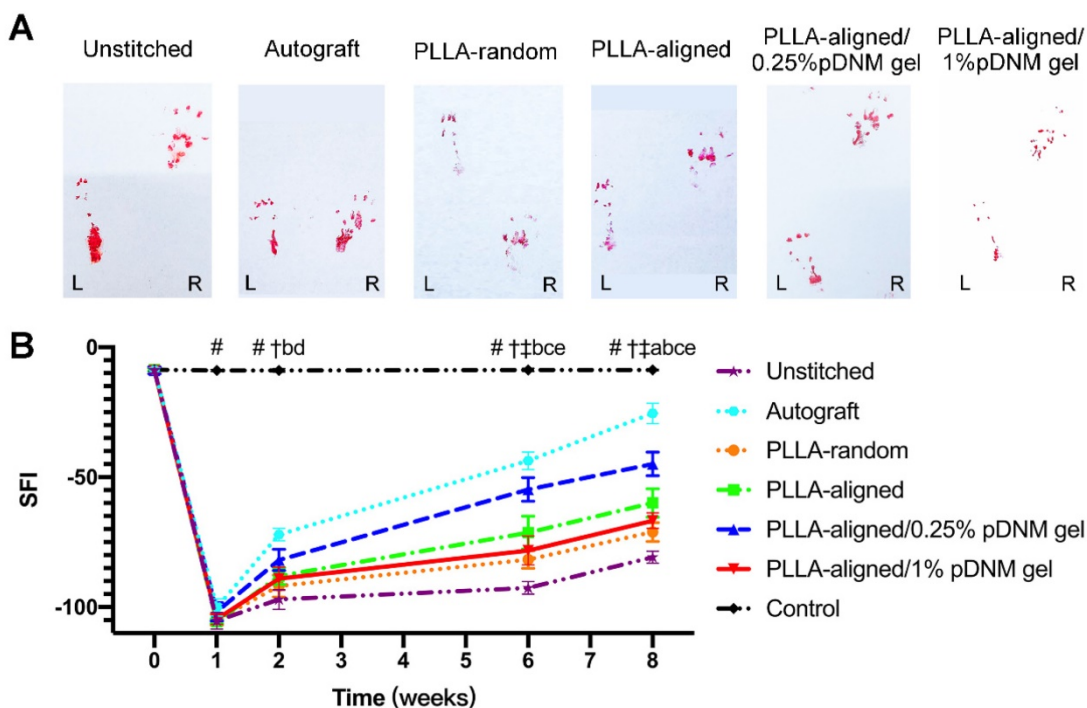


Figure 7. Walking track analysis of the sciatic nerve-injured rats. (A) Hind paw footprints of all injured groups at 8 weeks post-surgery. **(B)** Sciatic nerve function index (SFI) of the injured side compared with the contralateral uninjured side post-surgery. Statistically significant differences are listed in Table S5.

Discussion

NGCs with aligned micro- or nano-architectures possess remarkable assets for promoting peripheral nerve regeneration [46-48]. Surface topographical patterns are critical to neurite outgrowth, which not only triggers neurite formation but also serves as directional guidance for targeted axonal extension. NGCs made of electrospun nanofibers promote directed axonal extension owing to their anisotropic alignment, which serves as the topological guidance for nerve fiber growth as well as the migration of Schwann cells along the direction of axonal extension [23, 31, 32]. In this study, longitudinally aligned electrospun nanofibers effectively provided guidance for neural cells. Histological analysis showed that the aligned nanofibrous structure in the PLLA-aligned group was a potent stimulator for axonal regeneration compared to the randomly oriented nanofibers in the PLLA-random group. Furthermore, the myelin thickness of the PLLA-aligned group was $0.494 \pm 0.021 \mu\text{m}$ and $0.536 \pm 0.028 \mu\text{m}$ at 6 and 8 weeks post-surgery, respectively, whereas the myelin thickness of the PLLA-random group was $0.440 \pm 0.027 \mu\text{m}$ and $0.524 \pm 0.028 \mu\text{m}$. Nerve fiber remyelination was facilitated by the aligned nanofibers rather than the randomly oriented fibers ($p < 0.002$). As a result, implantation of NGCs composed of PLLA-aligned scaffolds performed more significant functional recovery than those composed of

PLLA-random.

Synthetic materials, such as PLLA [27], poly(ϵ -caprolactone) [24], and other copolymers [31], have been applied for fabrication of tissue-engineered nerve scaffolds due to their mechanical stability and reproducibility [6]. However, topological guidance provided by electrospun nanofibers alone cannot fully recapitulate or mimic the complex microenvironment of nerve cells due to their lack of structural ECM components and neurotrophic factors. Incorporation of ECM proteins (e.g., collagen, laminin, fibronectin) or growth factors (e.g., nerve growth factor) into electrospun nanofibers has been frequently investigated in recent years [27, 49-51]. NGCs fabricated using these composite materials often have limited capability for nerve functional restoration, either because of their inferior bioactivity or rapid release of the bioactive compounds from the nanofibers. It is widely realized that dECM biomaterials obtained directly from tissues or organs may reconstruct a well-defined physical and chemical microenvironment for cell survival and development, and determine morphogenesis, homeostasis, and stem cell differentiation in tissue repair [11]. A recent study verified that porcine peripheral nerve-derived dECM scaffolds can effectively suppress immunoreactions after implantation, which was mostly attributed to the elimination of cellular components [52]. After processing into a hydrogel, the resulting pDNM gel preserved most of the functional ECM components,

including glycosaminoglycans, collagens, laminin, and fibronectin, which actively promote neurite outgrowth [22, 37]. Furthermore, pDNM gel was shown to facilitate nerve fiber remyelination *in vitro* [37]. However, pDNM gel alone could neither provide enough mechanical robustness to enable implantation, nor topological guidance for directed axonal extension. Therefore, the combination of electrospun PLLA nanofibers and pDNM gel are beneficial for nerve regeneration, which was proven *in vitro* as well as *in vivo* in this study. We found that NGCs composed of PLLA-aligned/0.25% pDNM gel exhibited superior performance in repairing peripheral nerve defects in terms of axonal regeneration, extent of myelination, and functional recovery compared to either PLLA-aligned/1% pDNM gel conduits or NGCs composed of aligned PLLA nanofibers alone (without pDNM gel coating). These results reveal that the fully shielded nanofibrous structures in the PLLA-aligned/1% pDNM gel scaffold concealed the topological guidance, which led to attenuated nerve regeneration despite the increased pDNM gel concentration.

Multiparametric MRI was employed to assess the extent of axonal regeneration *in situ*. T2 and FA values can serve as sensitive indicators for detecting peripheral nerve injury, as well as appropriate tools for noninvasive monitoring of nerve regeneration. T2 hyperintensity of distal degenerating nerves is the result of increased water content, myelin turnover, vascular permeability, inflammatory mediators, and axonal and myelin breakdown products [53, 54]. Meanwhile, FA values, as the main quantitative parameters of DTI, are more strongly correlated with the density and diameter of axons, rather than the density and thickness of myelin [43]. Quantitative T2 values and DTI metrics can be further compared with histological results and behavioral assessments for a fuller picture of axonal regeneration. In this study, the T2 and FA values of injured nerves grafted with NGCs composed of PLLA-aligned/0.25% pDNM gel indicated accelerated nerve tissue recovery compared with those of the PLLA-aligned and PLLA-aligned/1% pDNM gel groups. As histological assessments showed that more neurites, thicker axons, and thicker myelin were evident within regenerating nerve fibers of the PLLA-aligned/0.25% pDNM gel group compared to the other grafted groups, the rapid recoveries of T2 and FA values were most likely due to promoted axonal regeneration. Notedly, the nerve defects did not fully recover in all groups by 8 weeks post-surgery based on the histological analysis. However, the T2 values returned to normal, or even lower than those of the control group (i.e., uninjured nerve on the contralateral side),

whereas the FA values were still much lower than normal in all grafted groups at 1 to 8 weeks after surgery. This result implies that the FA values were more sensitive than the T2 values for detecting nerve regeneration.

FA measures the degree of anisotropic diffusion, which reflects the degree of cell alignment within the nerve fiber tracts. The FA value varies from 0 to 1, where 0 represents isotropic diffusion and 1 represents complete anisotropy [55]. In previously reported nerve crush injury models, increased FA values were observed within 3 weeks after injury in rats, while it took 4 weeks for the FA value to begin increasing after sciatic nerve injury in rabbits [56, 57]. These time points indicate the termination of Wallerian degeneration and complete clearance of myelin and axon debris [43]. In this study, the FA values began to increase only after the first week post-surgery for all groups implanted with NGCs, which is when the damaged nerves entered the axonal regeneration phase. However, the FA values of the PLLA-aligned/0.25% pDNM gel group increased much faster than those of the other groups implanted with NGCs, especially at 6 to 8 weeks post-surgery. Though the final FA values did not reach the levels of the uninjured contralateral nerves or the autografted group, the PLLA-aligned/0.25% pDNM gel group was considerably close to complete recovery at 8 weeks. These FA value changes were consistent with the behavioral and histological results. Taken together, these findings suggest that MRI assessment may serve as a useful tool for evaluating PNI repair.

Conclusions

NGCs incorporating aligned electrospun nanofibers providing topological guidance combined with pDNM gel inducing biological cues were implanted into a defected sciatic nerve injury rat model. Multiparametric MRI including T2-mapping and DTI was used to dynamically monitor the extent of nerve regeneration. The aligned nanofibers exhibited excellent performance in triggering directed axonal extension compared with randomly oriented nanofibers. Surface decoration with pDNM gel at a relatively low concentration further promoted nerve regeneration, including the number of axons, continuity of the nerve fibers, remyelination, and functional recovery. This biomaterial scaffold combined with MRI assessment is a promising approach for neural tissue engineering and the treatment and diagnosis of PNI.

Abbreviations

PNI, peripheral nerve injury; NGC, nerve guidance conduit; pDNM, porcine decellularized

nerve matrix; PLLA, Poly(*L*-lactic acid); MRI, magnetic resonance imaging; FA, fractional anisotropy; SFI, sciatic nerve function index; dECM, decellularized extracellular matrix; DRG, dorsal root ganglion; SC, Schwann cell; DTI, diffusion tensor imaging; TFE, 2,2,2-trifluoroethanol; P(LLA-TMC), poly(*L*-lactic acid-co-trimethylene carbonate); T2WI, T2-weighted imaging; TR, repetition time; TE, echo time; FOV, field of view; NSA, number of signals averaged; EPI, echoplanar imaging; FA, fractional anisotropy; ROI, region of interest; DTT, diffusion tensor tractography; SPRR1A, small proline-rich protein 1A; NPL, normal print length; NTS, normal toe spread; NIT, normal intermediary toe spread; EPL, experimental print length; ETS, experimental toe spread; EIT, experimental intermediary toe spread.

Supplementary Material

Supplementary materials and methods, figures and tables. <http://www.thno.org/v11p2917s1.pdf>

Acknowledgments

This work was supported by National Natural Science Foundation of China (51903255 and U1801681), The Key Areas Research and Development Program of Guangdong (2019B020235001 and 2020B1111150003), Guangdong Province Universities and Colleges Pearl River Scholar Funded Scheme (2017), Guangdong Natural Science Foundation (2018A030313776), Science and Technology Program of Guangzhou City (201904010364), and Guangdong Innovative and Entrepreneurial Research Team Program (2013S086).

Author Contributions

J. S, Y. B, and D. Q conceived the experiments, critically reviewed the manuscript. Y. B, C. Z, Z. Y, and S. C prepared the manuscript. S. C designed and fabricated the NGCs, performed mechanical tests and in vitro experiments. Z. R and C. Z prepared the pDNM gel. C. Z, Z. Y, and F. Z performed the animal experiments. C. Z, Z. Y, S. C performed statistical analysis.

Competing Interests

The authors have declared that no competing interest exists.

References

- Chang B, Quan Q, Lu SB, Wang Y, Peng J. Molecular mechanisms in the initiation phase of Wallerian degeneration. *Eur J Neurosci*. 2016; 44: 2040-8.
- Deumens R, Bozkurt A, Meek MF, Marcus MA, Joosten EA, Weis J, et al. Repairing injured peripheral nerves: bridging the gap. *Prog Neurobiol*. 2010; 92: 245-76.
- Ray WZ, Mackinnon SE. Management of nerve gaps: autografts, allografts, nerve transfers, and end-to-side neurorrhaphy. *Exp Neurol*. 2010; 223: 77-85.
- Deumens R, Bozkurt A, Meek MF, Marcus MAE, Joosten EAJ, Weis J, et al. Repairing injured peripheral nerves: Bridging the gap. *Prog Neurobiol*. 2010; 92: 245-76.
- Gu X, Ding F, Yang Y, Liu J. Construction of tissue engineered nerve grafts and their application in peripheral nerve regeneration. *Prog Neurobiol*. 2011; 93: 204-30.
- Sarker MD, Naghieh S, McInnes AD, Schreyer DJ, Chen X. Regeneration of peripheral nerves by nerve guidance conduits: Influence of design, biopolymers, cells, growth factors, and physical stimuli. *Prog Neurobiol*. 2018; 171: 125-50.
- Bellamkonda RV. Peripheral nerve regeneration: an opinion on channels, scaffolds and anisotropy. *Biomaterials*. 2006; 27: 3515-8.
- Kehoe S, Zhang XF, Boyd D. FDA approved guidance conduits and wraps for peripheral nerve injury: A review of materials and efficacy. *Injury*. 2012; 43: 553-72.
- Gaudin R, Knipfer C, Henningsen A, Smeets R, Heiland M, Hadlock T. Approaches to peripheral nerve repair: generations of biomaterial conduits yielding to replacing autologous nerve grafts in craniomaxillofacial surgery. *Biomed Res Int*. 2016; 2016: 3856262.
- Jiang X, Lim SH, Mao HQ, Chew SY. Current applications and future perspectives of artificial nerve conduits. *Exp Neurol*. 2010; 223: 86-101.
- Choi J, Kim JH, Jang JW, Kim HJ, Choi SH, Kwon SW. Decellularized sciatic nerve matrix as a biodegradable conduit for peripheral nerve regeneration. *Neural Regen Res*. 2018; 13: 1796-803.
- Vijayaventaraman S. Nerve guide conduits for peripheral nerve injury repair: A review on design, materials and fabrication methods. *Acta Biomater*. 2020; 106: 54-69.
- Rao F, Wang YH, Zhang DY, Lu CF, Cao Z, Sui JJ, et al. Aligned chitosan nanofiber hydrogel grafted with peptides mimicking bioactive brain-derived neurotrophic factor and vascular endothelial growth factor repair long-distance sciatic nerve defects in rats. *Theranostics*. 2020; 10: 1590-603.
- Yang SH, Wang C, Zhu JJ, Lu CF, Li HT, Chen FY, et al. Self-assembling peptide hydrogels functionalized with LN- and BDNF- mimicking epitopes synergistically enhance peripheral nerve regeneration. *Theranostics*. 2020; 10: 8227-49.
- Gu XS, Ding F, Yang YM, Liu J. Construction of tissue engineered nerve grafts and their application in peripheral nerve regeneration. *Prog Neurobiol*. 2011; 93: 204-30.
- Schmidt CE, Leach JB. Neural tissue engineering: strategies for repair and regeneration. *Annu Rev Biomed Eng*. 2003; 5: 293-347.
- Panayi AC, Orgill DP. Current Use of Biological Scaffolds in Plastic Surgery. *Plast Reconstr Surg*. 2019; 143: 209E-20E.
- Mendibil U, Ruiz-Hernandez R, Retegi-Carrion S, Garcia-Urquia N, Olalde-Graells B, Abarregui A. Tissue-Specific Decellularization Methods: Rationale and Strategies to Achieve Regenerative Compounds. *Int J Mol Sci*. 2020; 21: 5447.
- Seo Y, Jung Y, Kim SH. Decellularized heart ECM hydrogel using supercritical carbon dioxide for improved angiogenesis. *Acta Biomater*. 2017; 67: 270-81.
- Hong JY, Seo Y, Davaa G, Kim HW, Kim SH, Hyun JK. Decellularized brain matrix enhances macrophage polarization and functional improvements in rat spinal cord injury. *Acta Biomater*. 2019; 101: 357-71.
- Zou JL, Liu S, Sun JH, Yang WH, Xu YW, Rao ZL, et al. Peripheral nerve-derived matrix hydrogel promotes remyelination and Inhibits synapse formation. *Adv Funct Mater*. 2018; 28: 1705739.
- Lin T, Liu S, Chen SH, Qiu S, Rao ZL, Liu JH, et al. Hydrogel derived from porcine decellularized nerve tissue as a promising biomaterial for repairing peripheral nerve defects. *Acta Biomater*. 2018; 73: 326-38.
- Yao L, O'Brien N, Windebank A, Pandit A. Orienting neurite growth in electrospun fibrous neural conduits. *J Biomed Mater Res B Appl Biomater*. 2009; 90: 483-91.
- He LM, Liao SS, Quan DP, Ma K, Chan C, Ramakrishna S, et al. Synergistic effects of electrospun PLLA fiber dimension and pattern on neonatal mouse cerebellum C17.2 stem cells. *Acta Biomater*. 2010; 6: 2960-9.
- Corey JM, Gertz CC, Wang BS, Birrell JK, Johnson SL, Martin DC, et al. The design of electrospun PLLA nanofiber scaffolds compatible with serum-free growth of primary motor and sensory neurons. *Acta Biomater*. 2008; 4: 863-75.
- Yang F, Murugan R, Wang S, Ramakrishna S. Electrospinning of nano/micro scale poly (*L*-lactic acid) aligned fibers and their potential in neural tissue engineering. *Biomaterials*. 2005; 26: 2601-10.
- Schnell E, Klinkhammer K, Balzer S, Brook G, Klee D, Dalton P, et al. Guidance of glial cell migration and axonal growth on electrospun nanofibers of poly-epsilon-caprolactone and a collagen/poly-epsilon-caprolactone blend. *Biomaterials*. 2007; 28: 3012-25.
- Corey JM, Lin DY, Mycek KB, Chen Q, Samuel S, Feldman EL, et al. Aligned electrospun nanofibers specify the direction of dorsal root ganglia neurite growth. *J Biomed Mater Res A*. 2007; 83: 636-45.
- Wang HB, Mullins ME, Cregg JM, Hurtado A, Oudega M, Trombley MT, et al. Creation of highly aligned electrospun poly-*L*-lactic acid fibers for nerve regeneration applications. *J Neural Eng*. 2009; 6: 016001.
- Chew SY, Mi R, Hoke A, Leong KW. The effect of the alignment of electrospun fibrous scaffolds on Schwann cell maturation. *Biomaterials*. 2008; 29: 653-61.
- Xia HJ, Sun XC, Liu D, Zhou YD, Zhong D. Oriented growth of rat Schwann cells on aligned electrospun poly(methyl methacrylate) nanofibers. *J Neurol Sci*. 2016; 369: 88-95.

32. Chen SH, Du ZY, Zou JL, Qiu S, Rao ZL, Liu S, et al. Promoting neurite growth and Schwann cells migration by harnessing decellularized nerve matrix onto nanofibrous guidance. *ACS Appl Mater Interfaces.* 2019; 11: 17167-76.
33. Guido S, Martin B, Jose P, Mirko P. Magnetic resonance imaging of the peripheral nervous system. *J Neurol.* 2009; 256: 1043-51.
34. Farinas AF, Pollins AC, Stephanides M, O'Neill D, Al-Kassis S, Esteve IVM, et al. Diffusion tensor tractography to visualize axonal outgrowth and regeneration in a 4-cm reverse autograft sciatic nerve rabbit injury model. *Neurol Res.* 2019; 41: 257-64.
35. Zheng CS, Zhang X, Chen YY, Zhang F, Duan XH, Chen MW, et al. Assessment of the synergic effect of immunomodulation on nerve repair using multiparametric magnetic resonance imaging. *Muscle Nerve.* 2018; 57: E38-E45.
36. Martin Noguerol T, Barousse R, Socolovsky M, Luna A. Quantitative magnetic resonance (MR) neurography for evaluation of peripheral nerves and plexus injuries. *Quant Imaging Med Surg.* 2017; 7: 398-421.
37. Zou JL, Liu S, Sun JH, Yang WH, Xu YW, Rao ZL, et al. Peripheral nerve-derived matrix hydrogel promotes remyelination and Inhibits synapse formation. *Adv Funct Mater.* 2018; 28: 1705739.
38. Liao CD, Zhang F, Guo RM, Zhong XM, Zhu J, Wen XH, et al. Peripheral nerve repair: monitoring by using gadofluorine M-enhanced MR imaging with chitosan nerve conduits with cultured mesenchymal stem cells in rat model of neurotmesis. *Radiology.* 2012; 262: 161-71.
39. Yang X, Xue P, Wei R, Liu X, Xu X, Liu ZY, et al. Dihydrotestosterone Treatment Accelerates Autograft Reversal Sciatic Nerve Regeneration in Rats. *Neurochemical Res.* 2018; 43: 659-68.
40. Jiang W, Wang Y, Tang J, Peng J, Wang Y, Guo Q, et al. Low-intensity pulsed ultrasound treatment improved the rate of autograft peripheral nerve regeneration in rat. *Sci Rep.* 2016; 6: 22773.
41. Yang ZH, Zheng CS, Zhang F, Lin BL, Cao MH, Tian XW, et al. Magnetic Resonance Imaging of Enhanced Nerve Repair with Mesenchymal Stem Cells Combined with Microenvironment Immunomodulation in Neurotmesis. *Muscle Nerve.* 2020; 61: 815-25.
42. Chen YY, Lin XF, Zhang F, Zhang X, Hu HJ, Wang DY, et al. Diffusion tensor imaging of symptomatic nerve roots in patients with cervical disc herniation. *Acad Radiol.* 2014; 21: 338-44.
43. Takagi T, Nakamura M, Yamada M, Hikishima K, Momoshima S, Fujiyoshi K, et al. Visualization of peripheral nerve degeneration and regeneration: monitoring with diffusion tensor tractography. *Neuroimage.* 2009; 44: 884-92.
44. Mekaj AY, Manxhuka-Kerliu S, Morina AA, Duci SB, Shahini L, Mekaj YH. Effects of hyaluronic acid and tacrolimus on the prevention of perineural scar formation and on nerve regeneration after sciatic nerve repair in a rabbit model. *Eur J Trauma Emerg Surg.* 2017; 43: 497-504.
45. Antonios JP, Farah GJ, Cleary DR, Martin JR, Ciacci JD, Pham MH. Immunosuppressive mechanisms for stem cell transplant survival in spinal cord injury. *Neurosurg Focus.* 2019; 46: E9.
46. Huang LL, Zhu L, Shi XW, Xia B, Liu ZY, Zhu S, et al. A compound scaffold with uniform longitudinally oriented guidance cues and a porous sheath promotes peripheral nerve regeneration in vivo. *Acta Biomater.* 2017; 68: 223-36.
47. Li GC, Xue CB, Wang HK, Yang XM, Zhao YX, Zhang LZ, et al. Spatially featured porous chitosan conduits with micropatterned inner wall and seamless sidewall for bridging peripheral nerve regeneration. *Carbohydr Polym.* 2018; 194: 225-35.
48. Singh A, Asikainen S, Teotia AK, Shiekh PA, Huotilainen E, Qayoom I, et al. Biomimetic Photocurable Three-Dimensional Printed Nerve Guidance Channels with Aligned Cryomatrix Lumen for Peripheral Nerve Regeneration. *Acc Appl Mater Inter.* 2018; 10: 43327-42.
49. Wu T, Li DD, Wang YF, Sun BB, Li DW, Morsi Y, et al. Laminin-coated nerve guidance conduits based on poly(*L*-lactide-co-glycolide) fibers and yarns for promoting Schwann cells' proliferation and migration. *J Mater Chem B.* 2017; 5: 3186-94.
50. Mukhatyar VJ, Salmeron-Sanchez M, Rudra S, Mukhopadaya S, Barker TH, Garcia AJ, et al. Role of fibronectin in topographical guidance of neurite extension on electrospun fibers. *Biomaterials.* 2011; 32: 3958-68.
51. Xia B, Lv YG. Dual-delivery of VEGF and NGF by emulsion electrospun nanofibrous scaffold for peripheral nerve regeneration. *Mat Sci Eng C-Mater.* 2017; 82: 253-64.
52. Crapo PM, Gilbert TW, Badylak SF. An overview of tissue and whole organ decellularization processes. *Biomaterials.* 2011; 32: 3233-43.
53. Chen P, Piao X, Bonaldo P. Role of macrophages in Wallerian degeneration and axonal regeneration after peripheral nerve injury. *Acta Neuropathol.* 2015; 130: 605-18.
54. Shen J, Zhou CP, Zhong XM, Guo RM, Griffith JF, Chen LN, et al. MR neurography: T1 and T2 measurements in acute peripheral nerve traction injury in rabbits. *Radiology.* 2010; 254: 729-38.
55. Jeon T, Fung MM, Koch KM, Tan ET, Sneag DB. Peripheral nerve diffusion tensor imaging: Overview, pitfalls, and future directions. *J Magn Reson Imaging.* 2018; 47: 1171-89.
56. Yamasaki T, Fujiwara H, Oda R, Mikami Y, Ikeda T, Nagae M, et al. In vivo evaluation of rabbit sciatic nerve regeneration with diffusion tensor imaging (DTI): correlations with histology and behavior. *Magn Reson Imaging.* 2015; 33: 95-101.
57. Morisaki S, Kawai Y, Umeda M, Nishi M, Oda R, Fujiwara H, et al. In vivo assessment of peripheral nerve regeneration by diffusion tensor imaging. *Magn Reson Imaging.* 2011; 33: 535-42.